Available online at www.sciencedirect.com
SCIENCE DIRECT®
Journal of Power Sources 132 (2004) 266–274
JOURNAL OF POWER SOURCES
www.elsevier.com/locate/jpowsour

Mathematic simulation on power generation by roll cake type of thermoelectric tubes

Ryosuke O. Suzuki [a,*], Daisuke Tanaka [b,1]

[a] *Department of Energy Science and Technology, Kyoto University, Yoshida-honmachi, Sakyo-ku, Kyoto 606-8501, Japan*
[b] *Graduate School of Energy Science, Kyoto University, Japan*

Received 27 June 2003; received in revised form 24 December 2003; accepted 5 January 2004

Abstract

Analytical expression of electric power was deduced in case of the large-scale thermoelectric device that consists of the multiple cylindrical tubes like roll cake exposed to two thermal fluids. The output powers of the four arrangements were mathematically solved from heat transfer theory. The maximum output power of roll-cake module was practically the largest for the system of the counter flow with a single thermoelectric tube (V1C system), but 1/4 of the ideal output power (V1II system). The multiplication of thermoelectric tubes can shorten significantly the device length, although the output power decreases only a little. For example, the double vortical tubes (V2CC system) can generate 95.7% output power by 38.5% diameter, compared with the single tube (V1C system).

Keywords: Thermoelectric generation; Thermoelectric device; Heat transfer; Thermal fluid; Bismuth telluride

1. Introduction

A thermal energy is supplied as a form of fluid in a large-scale thermoelectric power plant. When a hot fluid offers the heat to the hot junctions in the thermoelectric modules, the thermoelectric motive force (EMF) due to Seebeck effect is generated depending on a temperature difference between the hot and cold junctions. EMF in the open circuit is the sum of multiplication of the relative Seebeck coefficient and the temperature difference $\Delta\theta$ over all the serial connections. In order to gain the larger power, therefore, we give the larger $\Delta\theta$ to all the thermoelectric panels existing between two hot and cold fluids [1–4].

The heat applied from a hot fluid is transferred firstly to the panel surface, then into the thermoelectric panel, and finally to the cold fluid at another surface. The two fluids are resultantly warmed or cooled along the flow paths, and their temperature profiles through the path, $T(x)$, change as a function of position, x. This problem is known in heat exchanger through an isolator [5–7].

The previous studies showed that the maximum of output power exists corresponding to a certain module size [8–12]. It is because the longer serial connections of thermoelements can generate the higher voltage, but because the output power decreases both by the higher electrical resistance, and by the smaller temperature difference ΔT due to the higher heat transfer through the modules.

Our previous studies showed that the necessary panel area could be minimized when the thermoelectric multi-panels were connected three-dimensionally [11,12]. The helical system shown in Fig. 1 enables to shorten the panel length and makes the system more compact and suitable for the large-scale power generation. For example, the system of Fig. 1 consists of five thermoelectric panels, among which two hot fluids and the two cold fluids flow as counter flow. The cylindrical tubes consisting of the thermoelectric modules are suitable for circulation of the industrial fluids, such as exhaust hot gas or coolant water. Fig. 2 was the idea that made it practical to circulate the fluids as proposed in Fig. 1 [12]. We reported the mathematical expression of its output power using the heat transfer analysis. However, the practical arrangement of the multi-tubes causes the practical problems at the parts of tube connection, as shown in Fig. 2.

Fig. 3 shows another possibility to shorten the cylindrical thermoelectric tubes. The two fluids flow in the counter directions along the thermoelectric vortical walls, which looks like roll cake. The purpose of this work is to deduce the mathematical expression of the electric power extractible

* Corresponding author. Tel.: +81-75-753-5453; fax: +81-75-753-5432.
E-mail address: suzuki@energy.kyoto-u.ac.jp (R.O. Suzuki).
[1] Present address: Nomura Research Institute, Ltd. Tokyo, Japan.

0378-7753/$ – see front matter © 2004 Elsevier B.V. All rights reserved.
doi:10.1016/j.jpowsour.2004.01.018

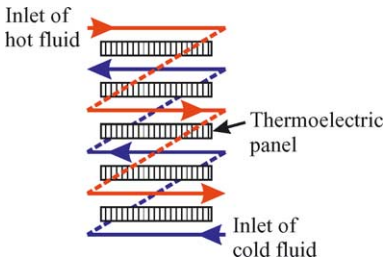

Fig. 1. Helical system with flat thermoelectric panels.

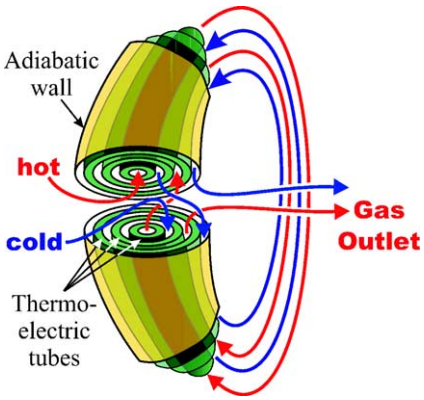

Fig. 2. Cylindrical multi-tube system with helical paths in which two fluids flow in the counter directions (T3CH type).

from the thermoelectric cylindrical tubes in case of Fig. 3 (Vortical system, V).

2. Basic assumptions and models

2.1. Directions and paths of fluids

The previous studies clarified that the parallel flow did not give the larger output than the counter flow, either in the flat panel systems (F system) [11] nor the cylindrical tube systems (T system) [12]. Therefore, the counter flow is mainly studied for the vortical systems (V system).

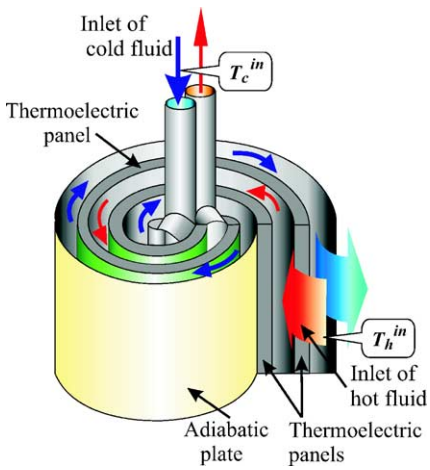

Fig. 3. Example of three-dimensional helical system (roll pan-cake model). V2CC system.

For easy mathematical handling, the roll cake systems (Figs. 4(a) and 5(a)) are simplified to the systems with the combined multi-cylinders (Figs. 4(b), (c) and 5(b)). When the inner radius of the inner tube, r_{11}, is enough large comparing with the path width, a, we may neglect the turbulent effects near the inlet and outlet. The analyzed vortical (V) systems are named after the number of thermoelectric tubes (n) and the direction of fluid flow (counter flow, "C", and parallel flow, "P"). Therefore, we call the three systems (Figs. 4(b), (c) and 5(b)) as V1C, V1P and V2CC system, respectively. For comparison, the case that the both surfaces of a tube are kept isothermally ("I") is also calculated as V1II system. The hydrodynamic conditions and the boundary conditions in these four mathematical models are listed in Table 1.

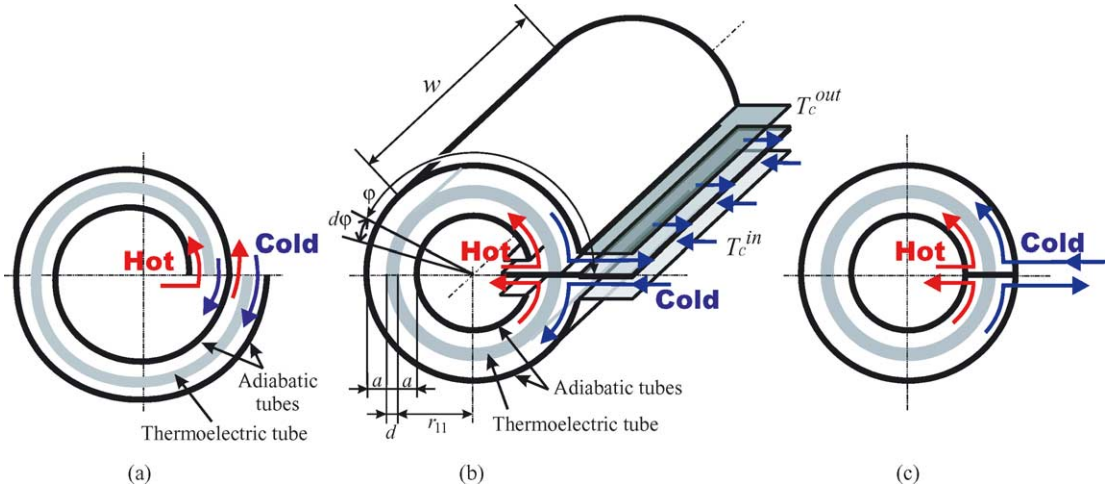

Fig. 4. Vortical systems with a cylindrical thermoelectric tube: (a) roll-cake model, (b) analyzed module (V1C), (c) analyzed module (V1P).

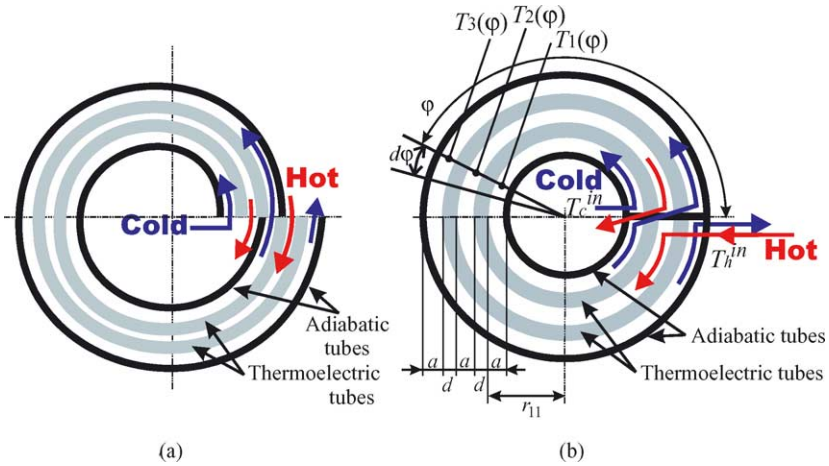

Fig. 5. Vortical systems with double cylindrical thermoelectric tubes: (a) roll-cake model, (b) analyzed module (V2CC).

Table 1
Conditions for the analyzed systems

System	Hydrodynamic conditions	Boundary conditions	Model
V1C	$M_1 > 0$, $M_2 < 0$	$T_1(0) = T_h^{in}$, $T_2(2\pi) = T_c^{in}$	Fig. 4(b)
V1P	$M_1 > 0$, $M_2 > 0$	$T_1(0) = T_h^{in}$, $T_2(0) = T_c^{in}$	Fig. 4(c)
V1II	$M_1 = \infty$, $M_2 = -\infty$	$T_1(\varphi) = T_h^{in}$, $T_2(\varphi) = T_c^{in}$ at any φ	
V2CC	$M_1 > 0$, $M_2 < 0$, $M_3 = M_1 > 0$	$T_1(0) = T_c^{in}$, $T_2(2\pi) = T_h^{in}$, $T_3(0) = T_1(2\pi)$	Fig. 5(b)

2.2. Cylindrical thermoelectric tube

It is assumed that all of our thermoelectric modules are cylindrically fan-shaped, and that they consist of the thermoelements with a single layer of Π-type p–n junctions, as illustrated in Fig. 6. The thermoelements are homogeneously aligned parallel to heat flow, combined tightly without open space, and connected electrically in series. The hot and cold fluids are isolated by this thermoelectric panel, and they flow along the both cylindrical surfaces of the panel in the direction of φ. Practically, as shown in Fig. 6(a), there exist the electrodes connecting the thermoelements, the insulator between the elements, the protective insulating film on the electrodes, and the fins that enhance the heat exchange. Here for simplicity, we neglected these inhomogeneous effects on heat transfer, and considered them only as the heat transfer coefficient, h, of the homogeneously smooth modules.

The p–n pairs of length, L, are aligned as illustrated in Fig. 6(b), in order to consider the heat transfer through the thermoelectric panel that depends on the angle, φ. This definition of alignment is deferent with that of the previous approach [12].

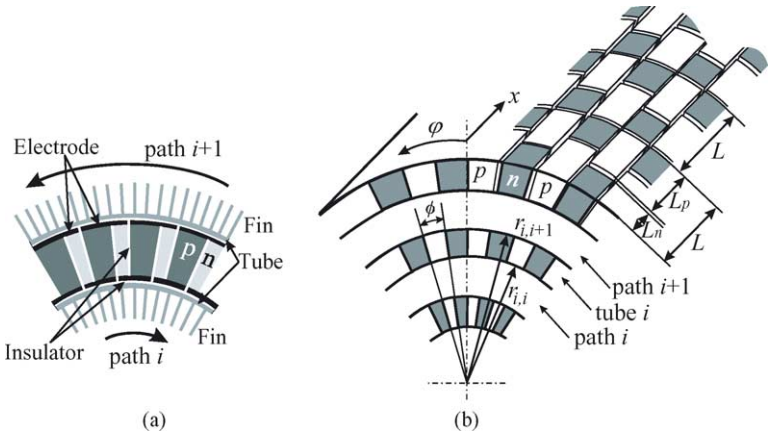

Fig. 6. Modeling of thermoelectric modules: (a) practical modules, (b) analyzed modules.

3. Equations for output power

3.1. Deduction of equations

Our previous analysis for multi-flat panels [11] is fundamentally applied for the multi-tubes. First we examine the heat transfer through the cylindrical thermoelectric tube [10,12]. The heat transfer coefficient K_i is calculated by building the local heat balance equations, considering that the heat transfer is not uniform, i.e. the fluid temperature depends on angle, φ. K_i is deduced here as the over-all heat transfer coefficient per unit length through the tube i in the direction perpendicular to r axis,

$$K_i = \frac{1}{(1/h_{i,i}r_{i,i}) + (\ln(r_{i,i+1}/r_{i,i})/\lambda) + (1/h_{i,i+1}r_{i,i+1})}. \quad (1)$$

$r_{i,j}$ and $h_{i,j}$ are the radius of the tube and the heat transfer coefficient between the tube i and the fluid j, respectively, and λ is the average heat conductivity of the module, defined by

$$\lambda = \frac{\lambda_p \times L_p + \lambda_n \times L_n}{L_p + L_n} = \frac{\lambda_p \times L_p + \lambda_n \times L_n}{L}, \quad (2)$$

where λ_p, λ_n, L_p and L_n are the heat conductivity and the length of p- and n-type elements, respectively. L is the unit length of thermoelectric pair, as shown in Fig. 6(b). Therefore, $L = L_p + L_n$. Note that K has been normally defined as the over-all heat transfer coefficient per unit length of the tube when the fluid flows along the tube length. K_i in our case is deduced when the fluid flows around the tube. As shown after the calculations, however, K_i can be replaced by $K/2\pi$ using the normal formula K.

Second, when the system consists of n tubes, a set of $n+1$ simultaneous derivative equations can be written from the heat transfers through tubes to obtain the fluid temperature, $T(\varphi)$, as a function of angle, φ. The homogeneous temperature along the tube length is assumed that the turbulent flow is well developed inside the long path.

$$M_1 C_{p,1} \frac{dT_1(\varphi)}{d\varphi} = \mp K_1 w(T_1(\varphi) - T_2(\varphi)), \quad (3)$$

$$M_i C_{p,i} \frac{dT_i(\varphi)}{d\varphi} = \pm K_{i-1} w(T_{i-1}(\varphi) - T_i(\varphi)) \mp K_i w(T_i(\varphi) - T_{i+1}(\varphi)), \quad (1 < i < n) \quad (4)$$

$$M_{n+1} C_{p,n+1} \frac{dT_{n+1}(\varphi)}{d\varphi} = \pm K_n w(T_n(\varphi) - T_{n+1}(\varphi)), \quad (5)$$

where M_i and $C_{p,i}$ are mass flow rate and heat capacity for fluid i, respectively. The choice of sign $\pm$ depends on the path condition. For simplicity, the heat transfer by Peltier effect and the exothermal heat by Joule effect are neglected. This assumption leads to an overestimation for output power, although this overestimation is not significant, as we will report separately.

Third, the temperature $\theta_{i,j}(\varphi)$ at the surface of the panel i facing to the fluid j is then written using the solutions of simultaneous derivative equations, $T_i(\varphi)$ for the angle φ

$$\theta_{i,i+1}(\varphi) - \theta_{i,i}(\varphi) = \frac{K_i}{\lambda}\{T_{i+1}(\varphi) - T_i(\varphi)\} \ln\left(\frac{r_{i,i+1}}{r_{i,i}}\right). \quad (6)$$

The electromotive force, E, is the summation of the temperature difference over all the panels.

$$E = \sum_{i=1}^{\text{panel}} \left| \frac{N_\phi n_x w \alpha}{2\pi} \int_0^{2\pi} (\theta_{i,i}(\varphi) - \theta_{i+1,i}(\varphi))\, d\varphi \right|, \quad (7)$$

where α is the difference between the Seebeck coefficients of p and n elements, N_ϕ and n_x are the number of thermoelectric pairs in a cylindrical circulation, and the number densities of pairs in the direction x, respectively. Therefore, $N_\phi = 2\pi/\phi$ and $n_x = 1/L$. ϕ is the circumferential angle of a pair, as shown in Fig. 6(b).

The electric resistance, R_i, is deduced by integrating the resistance of a thin fan-shaped layer in the direction of radius.

$$R_i = \frac{N_\phi{}^2 n_x w}{2\pi} \left(\frac{\rho_p}{L_p} + \frac{\rho_n}{L_n}\right) \ln\left(\frac{r_{i,i+1}}{r_{i,i}}\right), \quad (8)$$

where ρ_p and ρ_n are the specific resistivity of p and n elements. Eq. (8) neglects the resistance of electrode connecting p and n elements.

Finally, the output power, P, is optimized by balancing the internal and external resistance.

$$P = \frac{E^2}{4\sum_{i=1}^{\text{panel}} R_i}. \quad (9)$$

This work uses hereafter this P, where the internal resistance is equal to the external resistance.

3.2. Output power of V1C, V1P and V1II systems

The simultaneous equations are solved first at the V1C system, where one sheet of panel is exposed in counter flow. EMF and the output power are generally calculated by Eqs. (7) and (9) as,

$$E_{V1C} = \frac{n_x N_\phi M_1 M_2 C_{p,1} C_{p,2} \alpha (T_h^{in} - T_c^{in}) \ln(r_{12}/r_{11})}{2\pi\lambda} \times \left\{ \frac{\exp(2\pi K_1 wD) - 1}{M_1 C_{p,1} + M_2 C_{p,2} \exp(2\pi K_1 wD)} \right\}, \quad (10)$$

$$P_{V1C} = \frac{n_x \{M_1 M_2 C_{p,1} C_{p,2} \alpha (T_h^{in} - T_c^{in})\}^2 \ln(r_{12}/r_{11})}{8\pi w \lambda^2 ((\rho_n/L_n) + (\rho_p/L_p))} \times \left\{ \frac{\exp(2\pi K_1 wD) - 1}{M_1 C_{p,1} + M_2 C_{p,2} \exp(2\pi K_1 wD)} \right\}^2, \quad (11)$$

where

$$D = \frac{1}{M_1 C_{\mathrm{p},1}} + \frac{1}{M_2 C_{\mathrm{p},2}}. \tag{12}$$

When $M_1 C_{\mathrm{p},1} = -M_2 C_{\mathrm{p},2} = MC_{\mathrm{p}}(>0)$, the special care was needed in solving the differential equations. EMF and the output power of this case are,

$$E_{\mathrm{V1C}} = \frac{n_x N_\phi MC_{\mathrm{p}} K_1 w \alpha (T_h^{\mathrm{in}} - T_c^{\mathrm{in}}) \ln(r_{12}/r_{11})}{\lambda (MC_{\mathrm{p}} + 2\pi K_1 w)}, \tag{13}$$

$$P_{\mathrm{V1C}} = \frac{\pi n_x w \{MC_{\mathrm{p}} K_1 \alpha (T_h^{\mathrm{in}} - T_c^{\mathrm{in}})\}^2 \ln(r_{12}/r_{11})}{2\lambda^2 ((\rho_{\mathrm{n}}/L_{\mathrm{n}}) + (\rho_{\mathrm{p}}/L_{\mathrm{p}}))(MC_{\mathrm{p}} + 2\pi K_1 w)^2}. \tag{14}$$

They are equal to the infinite expressions of Eqs. (11) and (12), respectively, when $M_1 C_{\mathrm{p},1}$ approaches to $-M_2 C_{\mathrm{p},2}$.

The simultaneous equations are solved at the V1P system, where one sheet of panel is exposed in parallel flow. EMF and the output power are calculated as

$$E_{\mathrm{V1P}} = \frac{n_x N_\phi M_1 M_2 C_{\mathrm{p},1} C_{\mathrm{p},2} \alpha K_1 (T_h^{\mathrm{in}} - T_c^{\mathrm{in}}) \ln(r_{12}/r_{11})}{2\pi\lambda} \times \left\{ \frac{1 - \exp(-2\pi K_1 wD)}{M_1 C_{\mathrm{p},1} + M_2 C_{\mathrm{p},2}} \right\}, \tag{15}$$

$$P_{\mathrm{V1C}} = \frac{n_x \{M_1 M_2 C_{\mathrm{p},1} C_{\mathrm{p},2} \alpha (T_h^{\mathrm{in}} - T_c^{\mathrm{in}})\}^2 \ln(r_{12}/r_{11})}{8\pi w \lambda^2 ((\rho_{\mathrm{n}}/L_{\mathrm{n}}) + (\rho_{\mathrm{p}}/L_{\mathrm{p}}))} \times \left\{ \frac{1 - \exp(-2\pi K_1 wD)}{M_1 C_{\mathrm{p},1} + M_2 C_{\mathrm{p},2}} \right\}^2. \tag{16}$$

Resultantly, both the output power P_{V1C} and P_{V1P} are independent from the number of thermoelectric elements, N_ϕ. Second, the above-mentioned results are deduced for the situation that the hot and cold fluids flow inside and outside the thermoelectric tube, respectively, as illustrated in Fig. 4(b) and (c). However, these expressions, E_{V1C}, P_{V1C}, E_{V1P} and P_{V1P}, are the same for the opposite situations that the cold and hot fluids flow inside and outside the tube, respectively. Only a difference is the sign of EMF.

When both fluids are heated and cooled by the infinitely large heat sources, $T_1(\varphi)$ and $T_2(\varphi)$ are constantly equal to T_1^{in} and T_2^{in}, respectively, at any portion of the tube. This means that the flow rates of both fluids become infinite, i.e. $M_1 = |M_2| = \infty$. Mathematically, P_{V1II} is calculated from Eq. (9).

$$P_{\mathrm{V1II}} = \frac{\pi n_x w \{K_1 \alpha (T_h^{\mathrm{in}} - T_c^{\mathrm{in}})\}^2 \ln(r_{12}/r_{11})}{2\lambda^2 ((\rho_{\mathrm{n}}/L_{\mathrm{n}}) + (\rho_{\mathrm{p}}/L_{\mathrm{p}}))}. \tag{17}$$

3.3. Output power of V2CC system

In the V2CC system, we set $M_1 C_{\mathrm{p},1} = |M_2 C_{\mathrm{p},2}| = MC_{\mathrm{p}}$.

$$E_{\mathrm{V2CC}} = -N_\phi n_x MC_{\mathrm{p}} \alpha (T_h^{\mathrm{in}} - T_c^{\mathrm{in}}) \sinh(X) \times \left[\frac{(K_1 K_{a1} + K_2 K_{a2}) \cosh(X) + \sqrt{K_1 K_2}(K_{a1} - K_{a2}) \sinh(X)}{\sqrt{K_1 K_2} \cosh(2X) + (K_1 + K_2) \sinh(2X)} \right], \tag{18}$$

$$P_{\mathrm{V2CC}} = \frac{n_x L_{\mathrm{n}} L_{\mathrm{p}} \{MC_{\mathrm{p}} \alpha (T_h^{\mathrm{in}} - T_c^{\mathrm{in}}) \sinh(X)\}^2}{2\lambda w (L_{\mathrm{p}} \rho_{\mathrm{n}} + L_{\mathrm{n}} \rho_{\mathrm{p}})(K_{a1} + K_{a2})} \times \left[\frac{(K_1 K_{a1} + K_2 K_{a2}) \cosh(X) + \sqrt{K_1 K_2}(K_{a1} - K_{a2}) \sinh(X)}{\sqrt{K_1 K_2} \cosh(2X) + (K_1 + K_2) \sinh(2X)} \right]^2. \tag{19}$$

where K_{a1}, K_{a2} and X were defined as

$$K_{a1} = \frac{1}{\pi\lambda} \ln\left(\frac{r_{12}}{r_{11}}\right), \quad K_{a2} = \frac{1}{\pi\lambda} \ln\left(\frac{r_{23}}{r_{22}}\right), \tag{20}$$

$$X = \frac{\pi w \sqrt{K_1 K_2}}{MC_{\mathrm{p}}}, \tag{21}$$

respectively. The definitions of K_{a1} and K_{a2} are identical with the previous work [12]. The output power P_{V2CC} is also independent from the number of thermoelectric elements, N_ϕ. The obtained expressions of the output power contain a common term such as $n_x L_{\mathrm{n}} L_{\mathrm{p}} \{MC_{\mathrm{p}} \alpha (T_h^{\mathrm{in}} - T_c^{\mathrm{in}})\}^2 / \lambda (L_{\mathrm{p}} \rho_{\mathrm{n}} + L_{\mathrm{n}} \rho_{\mathrm{p}})$, however, the other parts depend complicatedly on the geometry of the system, electric resistivity and heat transfer coefficient K_i. Especially K_i depends on the radius of thermoelectric panel in the cylindrical system. This is unable to simplify our expressions, while the output power of the flat multi-panels systems could be expressed by the non-dimensional parameters [11]. Therefore, the obtained output power for four systems will be numerically compared using the thermophysical values of Bi_2Te_3 semiconductors.

4. Physical properties and conditions

The thermophysical properties of the BiTe thermoelectric elements in the literature scattered due to the impurities and the difference in preparation [1]. Table 2 shows a typical set

Table 2
Specific values of thermoelectric elements at room temperature [1]

Materials	Seebeck coefficient α (μV/K)	Resistivity ρ (μΩ m)	Thermal conductivity λ (W/K m)	Figure of merit Z (1/K)
Bi-54.3 at.% Te (p)	162	5.55	2.06	2.605×10^{-3}
Bi-64.5 at.% Te (n)	−240	10.1	2.02	

Table 3
Parameters for thermoelectric power generation system

	Variables	Values used in this work
Thermoelectric device	Length, w	Variable (typically 2 m)
	Thickness of tube, d	0.05 m
	Inner radius of inner tube, r_{11}	Variable (typically 2.347 m)
	Distance between two tubes, a (thickness of fluid path)	0.1 m
	Number density of pairs, n_x	50 m^{-1}
	Number of pairs round a circumferential cycle, N_ϕ	100
Thermal sources	Hot source	N_2 gas (inlet $T_h^{in} = 500$ K)
	Cold source	N_2 gas (inlet $T_c^{in} = 300$ K)
Gas properties	Specific heat, $C_{p,hot} = C_{p,cool}$	1044 J/kg K (at 400 K, 0.1 Pa)
	Mass flow rate, $M_{hot} = M_{cool}$	Variable (typically 1 kg/s)
	Heat transfer coefficient, $h_{hot} = h_{cool}$	500 W/m^2 K

of properties for an identical sample at room temperature [1], and used for this work. Table 3 shows the fluid properties and the parameters for thermoelectric tubes. These values are identical with our previous studies [10–12]. The thickness of thermoelectric elements was set as 0.05 m based on the previous discussion [12]. The path width (the gap between cylindrical two tubes) was set to be 0.1 m.

5. Numerical comparison of systems

5.1. Maximum output power in V1C system

The strict maximum of Eqs. (11), (14), (16) and (18) are deduced as a function of the ratio L_n/L_p, but not taken here because all the equations hereafter become the longer and complex mathematical expressions, even if we can neglect the dependency of K_1. The output P_{V1C} can be approximately maximized using the well-known conditions that

$$L_n = \frac{\sqrt{\lambda_p \times \rho_n}}{\sqrt{\lambda_n \times \rho_p} + \sqrt{\lambda_p \times \rho_n}} L, \quad \text{and}$$
$$L_p = \frac{\sqrt{\lambda_n \times \rho_p}}{\sqrt{\lambda_n \times \rho_p} + \sqrt{\lambda_p \times \rho_n}} L. \tag{22}$$

The strict solution for the maximum was not far from that by Eq. (22), when we used the numerical data mentioned in Section 4. The difference in output power was only within 0.003%, mainly because the difference between λ_n and λ_p was small. The optimized conditions for L_n and L_p (Eq. (22)) are used in the following calculations as a good approximation.

Figs. 7 and 8 show the output power thus evaluated for V1C system, where the flow rate of the fluids, M_1 and M_2, are set to be commonly 1 kg/s under the restriction of Eq. (22). The output power has the maximum at a certain length or a certain radius. The optimum tube length is given analytically as $w^{opt.} = MC_p/2\pi K_1$ when the inner radius r_{11} is fixed. For example, Fig. 7 shows that the maximum output power, P^{max}, is 5.467 kW at the optimum tube length $w^{opt.} = 2.510$ m when $r_{11} = 2$ m. When $w^{opt.} = MC_p/2\pi K_1$ in the V1C system ($M_1C_{p,1} = |M_2C_{p,2}| = MC_p$), Eq. (14) gives the maximum output power, P^{max}.

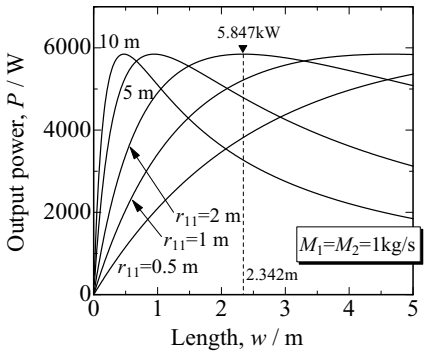

Fig. 7. Output power from V1C system as a function of tube length, w. r_{11} is the inner radius.

$$P_{V1C}^{max} = \frac{n_x MC_p K_1 \{\alpha(T_h^{in} - T_c^{in})\}^2 \ln(r_{12}/r_{11})}{16\lambda^2((\rho_n/L_n) + (\rho_p/L_p))} \tag{23}$$

The optimum radius $r_{11}^{opt.}$ when w is fixed, however, cannot be solved analytically. Numerically $P^{max} = 5.847$ kW is obtained at $r_{11}^{opt.} = 2.347$ m when $w = 2$ m (Fig. 8).

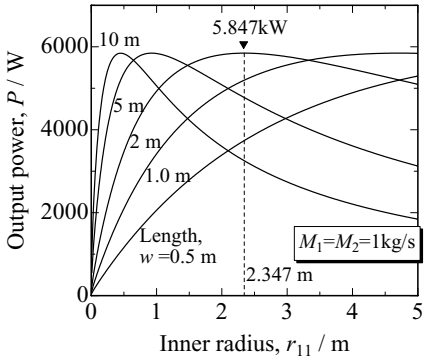

Fig. 8. Output power from V1C system as a function of inner radius, r_{11}.

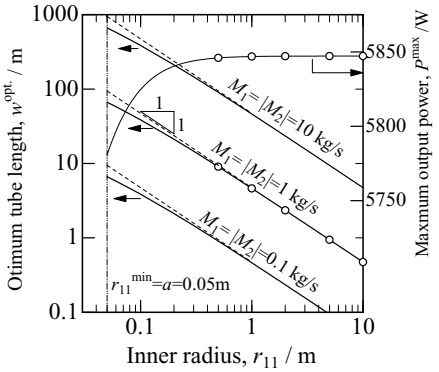

Fig. 9. Optimum tube length, $w^{opt.}$, for the given inner radius, r_{11}, and mass flow rates, M_1 and M_2. Maximum output power is shown only for $M = 1$ kg/s. Open circles show the optimum points shown in Fig. 7.

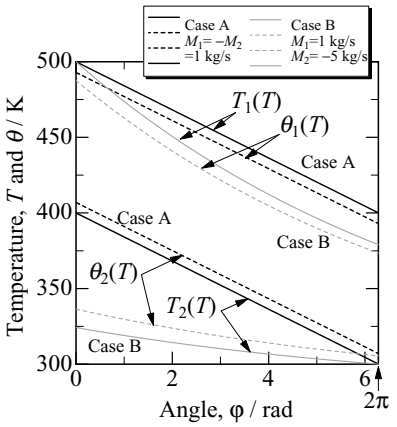

Fig. 10. Temperature profile along the tube in V1C system. T_1 and T_2 are temperatures of the fluids, and θ_1 and θ_2 are surface temperatures of the module, respectively. The inner radius and the tube length are set as $r_{11} = 2.347$ m and $w = 2$ m, respectively, for the both cases A and B.

The existence of the maximum output power was also reported in the flat panels and the cylindrical tubes [8–12]. It is qualitatively because the longer thermoelectric panel can generate the higher voltage, but because it increases the electrical resistance and decreases the temperature difference ΔT between the fluids. It is interesting that the values of P^{max} are nearly constant as shown in Fig. 9, even if the length and radius are varied. This is because K_1 changes linearly at $r_{11} > 1$ m.

5.2. Optimum dimension of V1C system

The relationship between the optimum length, $w^{opt.}$, and the optimum radius, $r_{11}^{opt.}$, to obtain P^{max} is analyzed in Fig. 9. $w^{opt.}$ changes linearly with r_{11}, although a small deviation from the linear regression is found at $r_{11} < 1$ m. This linearity means that there exists a certain optimum surface area, $S^{opt.} = 2\pi r_{11}^{opt.} w^{opt.}$ at a given flow rate. For example, $S^{opt.} = 29.8\,m^2$ and $P^{max} = 5.847$ kW for $M = 1$ kg/s and $r_{11} = 10$ m. This constant $S^{opt.}$ shows again that the cylindrical tube can be approximated as the flat panel at $r_{11} > 1$ m, because the previous work on the flat panel reported that the optimum surface size exists at the given flow conditions [11].

When r_{11} is smaller, however, the flat panel approximation is not valid because K_1 given in Eq. (1) does not depend linearly on r_{11}. For example, $w^{opt.} = 51.48$ m and $S^{opt.} = 22.6\,m^2$ for $r_{11} = 0.07$ m, where $P^{max} = 5.807$ kW. If we compare this case with the case of $r_{11} = 10$ m as mentioned above, P^{max} decreases only by 0.68% although $S^{opt.}$ decreases by 24.2%. Thus, the cylindrical tube with $r_{11} < 1$ m can generate the power more effectively per an unit surface than the flat panel, and we can save the number of modules necessary for power generation using the condition $r_{11} < 1$ m, without dropping P^{max}.

5.3. Temperature profiles in V1C system

Fig. 10 shows the temperatures, $T(\varphi)$ and $\theta(\varphi)$, on the tube surface in the V1C system. The temperature of the fluids $T_1(\varphi)$ and $T_2(\varphi)$ change linearly from the inlet to the outlet, when $M_1 C_{p,1} = |M_2 C_{p,2}| = MC_p$. When the maximum output is extracted from the optimum arrangements for the length and the inner radius (case A), the temperature difference between $T_1(\varphi)$ and $T_2(\varphi)$ is constant, i.e. $\Delta T(\varphi) = (T_1^{in} - T_2^{in})/2$, independent from φ, MC_p and K_1, and the outlet temperatures are $T_1^{out} = T_2^{out} = (T_1^{in} + T_2^{in})/2$.

Because of the thermal resistance at the surfaces, the temperature difference applied to the thermoelectric modules, $\Delta\theta(\varphi)$ $(= \theta_1(\varphi) - \theta_2(\varphi))$, is smaller than $\Delta T(\varphi)$. As seen in Eq. (7), the output power is proportional to the integral of $\Delta\theta(\varphi)$, which is visualized as the area A surrounded by $\theta_1(\varphi)$ and $\theta_2(\varphi)$ in Fig. 10. When the feeding rate of cold fluid $|M_2|$ becomes, for example, five times larger (case B), this area A expands as shown in Fig. 10. This is because the cold fluid decreases the temperature $\theta_2(\varphi)$, while the hot fluid is cooled and $\theta_1(\varphi)$ decreases. In total, the output power increases when the cold flow rate increases.

Fig. 11 shows the dependency of fluid flow rates on the output power, using Eq. (11). P_{V1C} increases when M_1 and

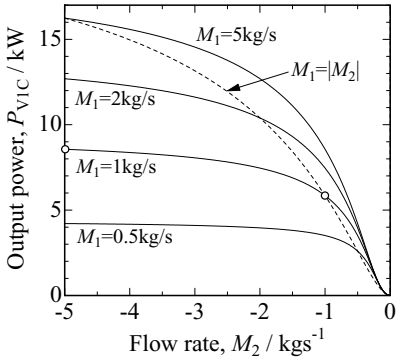

Fig. 11. Output power from V1C system as a function of flow rate of hot fluid, M_1, where $w = 2$ m and $r_{11} = 2.347$ m. Open circles show the data used in Fig. 10.

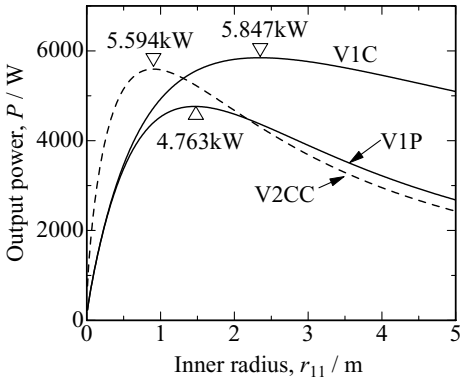

Fig. 12. Comparison of three systems, where the tube length $w = 2\,\mathrm{m}$ and the flow rate $|M| = 1\,\mathrm{kg/s}$ commonly. The triangles show the positions of maximum output power.

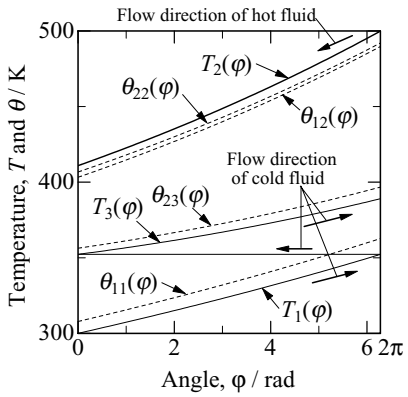

Fig. 13. Temperature profile along the tube in V2CC system. T_1, T_2 and T_3 are temperatures of the fluids, and θ_{11}, θ_{12}, θ_{22}, and θ_{23} are the surface temperatures of the module. $w = 2\,\mathrm{m}$ and $r_{11} = 2.347\,\mathrm{m}$.

$|M_2|$ increase. The largest $P^{\max} = 23.392\,\mathrm{kW}$ is obtained at the V1II system ($w = 2\,\mathrm{m}$, $r_{11} = 2.347\,\mathrm{m}$) where the flow rates of both fluids become infinite, i.e. $M_1 = |M_2| = \infty$, and $T_1(\varphi)$ and $T_2(\varphi)$ are equal to T_1^{in} and T_2^{in}, respectively, at any portion of the tube. P_{V1II} in Eq. (17) is exactly four times larger than $P_{\mathrm{V1C}}^{\max}$ given in Eq. (23) at $w^{\mathrm{opt.}}$. It is obviously because the area A becomes two times larger.

5.4. Maximum output power in V1P and V2CC systems

Fig. 12 shows the output power for three systems, where the flow rates of the fluids, $|M_i|$, are set to be commonly 1 kg/s and $w = 2\,\mathrm{m}$. The output power has the maximum also for V1P and V2CC systems. $P^{\max}$ was the largest for V1C system, while the optimum inner radius, $r_{11}^{\mathrm{opt.}}$, are 1.465 and 0.903 m for V1P and V2CC systems, respectively, shorter than $r_{11}^{\mathrm{opt.}}$ for V1C system (2.347 m). The fact that $P_{\mathrm{V1C}}^{\max}$ was larger than $P_{\mathrm{V1P}}^{\max}$ is consistent with the flat multi-panels and multi-tubes [11,12].

$P_{\mathrm{V2CC}}^{\max}$ was 95.7% of $P_{\mathrm{V1C}}^{\max}$, while $r_{11\,\mathrm{V2CC}}^{\mathrm{opt.}}$ was only 38.5% of $r_{11\,\mathrm{V1C}}^{\mathrm{opt.}}$. The inner surface of V2CC system per unit tube length when optimized ($2\pi(r_{11}^{\mathrm{opt.}} + r_{22}^{\mathrm{opt.}}) = 12.29\,\mathrm{m}$) is smaller than that of V1C ($2\pi r_{11}^{\mathrm{opt.}} = 14.75\,\mathrm{m}$). From the viewpoint of the more compact system to reduce the required modules and the space, the multiple tube system is more effective, and the V2CC system seems the most economic for construction. This tendency is similar with the systems with the multiple flat-panels or multi-tubes [11,12]. The multi-tubes systems such as V3CC or V4CC systems seem worth for further consideration.

5.5. Temperature profiles in V2CC system

Fig. 13 shows the temperatures, $T(\varphi)$ and $\theta(\varphi)$, on the tube surface for the case of the maximum output in the V2CC system. The temperatures of the fluids $T(\varphi)$ change exponentially from the inlet to the outlet, even if $M_1 C_{\mathrm{p},1} = |M_2 C_{\mathrm{p},2}| = M_3 C_{\mathrm{p},3} = MC_{\mathrm{p}}$. The hot fluid 2 is cooled from the both sides by the coolant, but the outlet temperature $T_2(0)$ for V2CC is higher than that for V1C (400 K, see Fig. 10). Because the preheated coolant in the path 1 is again circulated to the path 3, the temperature increment in the path 3, $T_3(2\pi) - T_3(0)$, is not so significant as that in the path 1, $T_1(2\pi) - T_1(0)$. The area A_1 surrounded by $\theta_{12}(\varphi)$ and $\theta_{11}(\varphi)$ is smaller than the area A_2 surrounded by $\theta_{22}(\varphi)$ and $\theta_{23}(\varphi)$, although $A_1 + A_2$ is proportional to EMF.

In this study, we have assumed that the whole panels are electrically connected in series. However, we may maximize additionally the output power by connecting them separately to the external circuits. This possibility will be reported separately.

6. Conclusion

This work studied the thermoelectric power generation with cylindrical multi-tubes in which thermoelectric elements were embedded. The fluid path connections were planed to be like roll-cake. Four systems were analyzed using the heat transfer theory, and their output powers were expressed in the analytical mathematic equations.

The maximum output power, $P^{\max}$, was obtained at the V1II system where the both surfaces of the tube were kept isothermally by the infinitively large heat sink. $P_{\mathrm{V1C}}^{\max}$ was the largest in the other three realistic systems, although the tube surface area necessary for the maximum output power was larger than V1P and V2CC system. When the radius of V1C system r_{11} becomes larger, its output approaches that of the flat panel, where an optimum surface area generates the maximum output power. The smaller r_{11} and the longer w generates the power more efficiently in V1C system. The V2CC system can generate the 95.7% power of that of V1C system, and $r_{11\,\mathrm{V2CC}}^{\mathrm{opt.}}$ is 38.5% of $r_{11\,\mathrm{V1C}}^{\mathrm{opt.}}$.

Acknowledgements

The authors thank to Mr. Hiroshi Hattori for his assistance. This work was supported in part by Japan Nuclear Cycle Development Institute (JNC), Yazaki Memorial Foundation for Science and Technology, and Sekisui Chemical Co. Ltd.

References

[1] R. Sakata (Ed.), Thermoelectrics, Principles and Applications, Realize Inc., Tokyo, 2001.
[2] K. Ono, R.O. Suzuki, R. Nakahashi, M. Shoda, Tetsu-to-Hagané 83 (1997) 157–161.
[3] K. Ono, R.O. Suzuki, in: Proceedings of the 17th International Conference on Thermoelectrics, IEEE, Piscataway, NJ, 1998, pp. 515–518.
[4] K. Ono, R.O. Suzuki, J. Metals December (1998) 49–51.
[5] S. Isshiki, N. Kitayama, Technology of Heat Transfer, Morikita Press, Tokyo, 1984.
[6] W.M. Kays, M.E. Crawford, Convective Heat and Mass Transfer, 2nd ed., McGraw-Hill, NY, 1980.
[7] Heat Transfer, 4th ed., Jpn. Soc. Mech. Eng., Tokyo, 1986.
[8] B. Mathiprakasam, T. Sutikno, J. Beeson, in: Proceedings of the 4th International Conference on Thermoelectrics, IEEE, Piscataway, NJ, 1982, p. 61.
[9] J. Esarte, G. Min, D.M. Rowe, J. Power Sources 93 (2001) 72–76.
[10] T. Kyono, R.O. Suzuki, K. Ono, IEEE Trans. Energy Conversion 18 (2003) 330–334.
[11] R.O. Suzuki, D. Tanaka, J. Power Sources 122 (2003) 201–209.
[12] R.O. Suzuki, D. Tanaka, J. Power Sources 124 (2003) 293–298.